

Revisiting the Generic Transformer: Deconstructing a Strong Baseline for Time Series Foundation Models

Yunshi Wen¹ Wesley M. Gifford² Chandra Reddy² Lam M. Nguyen²
Jayant Kalagnanam² Anak Agung Julius¹

Abstract

The recent surge in Time Series Foundation Models has rapidly advanced the field, yet the heterogeneous training setups across studies make it difficult to attribute improvements to architectural innovations versus data engineering. In this work, we investigate the potential of a standard patch Transformer, demonstrating that this generic architecture achieves state-of-the-art zero-shot forecasting performance using a straightforward training protocol. We conduct a comprehensive ablation study that covers model scaling, data composition, and training techniques to isolate the essential ingredients for high performance. Our findings identify the key drivers of performance, while confirming that the generic architecture itself demonstrates excellent scalability. By strictly controlling these variables, we provide comprehensive empirical results on model scaling across multiple dimensions. We release our open-source model and detailed findings to establish a transparent, reproducible baseline for future research.

1. Introduction

The recent shift from domain-specific models to cross-domain Time Series Foundation Models (TSFMs) capable of zero-shot generalization marks a significant advancement in the field. These models have demonstrated remarkable success across a diverse range of domains and downstream tasks (Godahewa et al., 2021; Jiang et al., 2023; Emami et al., 2023; Liu et al., 2023; Nguyen et al., 2023), achieving performance that matches or exceeds state-of-the-art (SOTA) supervised methods (Goswami et al., 2024; Wen et al., 2024; Shi et al., 2025). Given the ubiquity of time series data and the proven feasibility of this approach, TSFMs have garnered substantial attention in the recent literature.

¹Rensselaer Polytechnic Institute ²IBM Research. Correspondence to: Yunshi Wen <weny2@rpi.edu>.

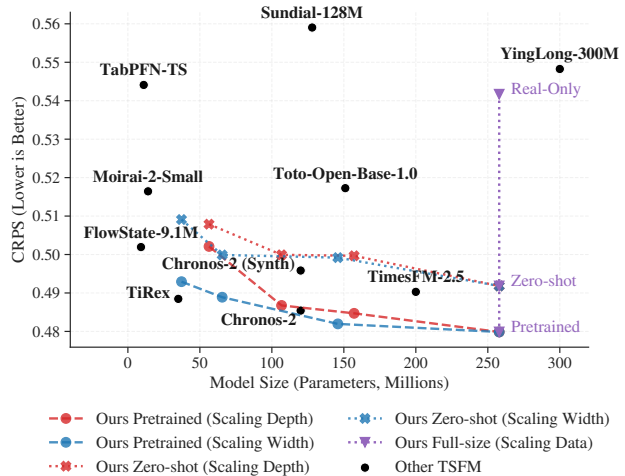


Figure 1. The Landscape of Time Series Foundation Models on Probabilistic Forecasting. We compare our generic Transformer with SOTA TSFMs on the GIFT-Eval benchmark. The results establish a strong baseline for neural scaling in TSFMs, and reveals that scaling in pretraining data is the primary driver of performance.

This surge of studies in the field of TSFMs, however, has introduced a confounding factor: heterogeneity in training protocols. Existing studies vary significantly in several aspects, including pretraining data composition, processing techniques, etc. This variability makes it difficult to attribute performance improvements to architectural innovations versus differences in data engineering. As the community explores diverse architectural designs, this lack of standardized training protocols in the comparison process obscures the actual contribution of novel architectures to the overall performance of TSFMs.

In this work, we demonstrate that a generic Patch Transformer architecture, when coupled with a straightforward training recipe, achieves state-of-the-art (SOTA) performance on the GIFT-Eval probabilistic forecasting benchmark (Aksu et al., 2025). Following this finding, we investigate the fundamental question: *What are the essential drivers of this effectiveness?* To answer this, we conduct a comprehensive empirical study to isolate the critical ingre-

dients required for a successful TSFM.

As illustrated in Figure 1, we compare the scaling behavior of our generic Patch Transformer against recent SOTA TSFMs. We observe that this standard architecture delivers performance comparable to, and sometimes exceeding, deliberately designed TSFMs across various model sizes. Notably, the visualization identifies that the enrichment of pretraining data composition serves as the primary driver of performance gains in TSFMs.

Our contributions are summarized as follows:

- **SOTA Performance with Generic Architecture:** We demonstrate that a standard Transformer architecture, utilizing patched inputs and quantile outputs, achieves state-of-the-art performance on the GIFT-Eval zero-shot forecasting leaderboard. This result serves as a strong evidence for the effectiveness of generic, scalable backbones.
- **Comprehensive Component Analysis:** We conduct a systematic ablation study to isolate the impact of critical training components, including model scaling laws, pretraining data composition, and training techniques. With comprehensive empirical experiments on each aspect, we unveil the essential ingredients for the success of TSFM.
- **Key Insights and Analysis:** Our analysis identifies pretraining data composition as an essential factor where both real-world and synthetic datasets contribute to a successful TSFM. We also provide extensive empirical evidence detailing how other key aspects affect the zero-shot performance of TSFM, including model scaling, contiguous patch masking, context length.
- **Open Research**¹: We release our pretrained model checkpoints, complete training pipeline, and detailed empirical results. By providing a transparent and reproducible baseline, we aim to facilitate fair comparisons and accelerate future research in TSFMs.

Scope of this Work: To ensure clarity and rigor, we define the scope of our study as follows:

- **Univariate Modeling and Zero-Shot Forecasting:** Our primary evaluation metric is zero-shot performance on univariate time series forecasting tasks. Specifically, our study focuses on the recipe of training a high-quality base foundation model. Therefore, no adaptation approaches, such as finetuning or agentic methods, are compared.
- **Ablation of Intrinsic Factors:** We focus exclusively on analyzing the scaling behaviors and component contributions within our proposed generic architecture. Rather than attempting to reproduce and retrain alternative architectures, which introduces significant variance due to differing implementations and resource requirements, we prioritize a controlled, in-depth analysis of the standard

Transformer to establish a robust baseline for the field.

2. Related Work

To consume large-scale pretraining data, TSFMs adopt scalable architectures paired with explicit input processing or “tokenization” strategies. Following its success in computer vision and natural language processing, the Transformer architecture (Vaswani et al., 2017) also serves as the dominant backbone choice for TSFMs. For time series data, tokenization approaches can vary between timestamp-level and patch-level granularities.

For instance, Chronos (Ansari et al., 2024) discretizes values at the timestamp level to construct a “language of time series,” enabling forecasting via a decoder-only autoregressive Transformer. TimesFM (Das et al., 2024) and Moirai (Woo et al., 2024) adopt patch-level tokenization to capture local semantics and improve computational efficiency, utilizing decoder-only and encoder-only (i.e., full-attention Transformer with masked inputs) architectures, respectively. Very recently, Chronos-2 (Ansari et al., 2025) extends the field from univariate TSFM to generic multivariate modeling and forecasting, while heavily relying on synthetic data. Beyond deterministic mapping, Sundial (Liu et al., 2025) integrates patch-level modeling with flow-matching decoding to provide more “natural” probabilistic forecasts from point predictions.

Recent works also explore state-space models as alternatives to the Transformer backbone, achieving high performance with relatively compact models. For example, Tirez (Auer et al., 2025) combines patch-level processing with the xLSTM (Beck et al., 2024) architecture. FlowState (Graf et al., 2025) formulates timestamp-level inputs as a discrete ODE using an S5 backbone (Smith et al., 2023), utilizing a specialized scaling factor to handle various sampling rates.

However, while these models continue to rapidly advance the SOTA results, their heterogeneous training protocols obscure the attribution of these gains. In particular, the increasing reliance on proprietary synthetic data generation pipelines, where the exact synthetic corpus is often not publicly released, introduces a significant uncontrolled variable. Consequently, it remains unclear whether recent improvements stem from the core architectural innovations or from superior data engineering (see Appendix B.2 for details).

3. Architecture

In this section, we present the formulation of our Time Series Foundation Model (TSFM) architecture, as illustrated in Figure 2. Our design leverages a standard Transformer backbone augmented with specific data processing and training techniques designed to enhance zero-shot generalization.

¹<https://huggingface.co/ibm-research/patchst-fm-r1>

3.1. Problem Formulation

Let $\mathbf{x} \in \mathbb{R}^T$ denote a univariate input time series of length T . To perform probabilistic predictions, our architecture takes x as input and predicts a set of quantiles $\hat{\mathbf{q}} \in \mathbb{R}^{T \times K}$ representing the distribution of the target values. This enables the model to capture the inherent uncertainty in time series data via a deterministic mapping.

To form semantically-meaningful tokens from real-value inputs, the time series \mathbf{x} is segmented into non-overlapping patches $\mathbf{p} \in \mathbb{R}^{N \times L}$, where L is the patch size and $N = \frac{T}{L}$ denotes the number of patches (Nie et al., 2023). Note that we pad or truncate the raw inputs to make a constant length T that is always divisible by L .

3.2. Contiguous Patch Masking

Contiguous Patch Masking (CPM) (Auer et al., 2025) encourages the model to learn long-horizon semantic dependencies rather than relying on local interpolation, thereby improving downstream performance on long-term forecasting tasks.

We define a binary mask $\mathbf{m} \in \{0, 1\}^T$, where $m_t = 1$ indicates a masked observation and $m_t = 0$ indicates a visible observation. Unlike the conventional approaches that uniformly sample scattered masks (He et al., 2022; Woo et al., 2024), CPM selects random starting positions (multiples of L) and masks blocks of $N_{\text{cpm}} \cdot L$ consecutive observations, as illustrated by the blue shaded regions in Figure 2. This creates substantial ‘‘information gaps’’ between the visible context and the targets, compelling the model to learn the underlying dynamics of the time series to bridge these gaps.

3.3. Mask-Aware Normalization

Heterogeneous value distribution and non-stationarity are major challenges in time-series modeling, where Reversible Instance Normalization (Kim et al., 2022) is proposed to mitigate such issues. In our masked autoencoding formulation, computing statistics including the masked (target) values would introduce information leakage about the target distribution.

To address this, we utilize Mask-Aware Normalization, which computes the mean μ and standard deviation σ using only the visible time points:

$$\mu = \frac{\sum_{t=1}^T \mathbb{1}(m_t = 0)x_t}{\sum_{t=1}^T \mathbb{1}(m_t = 0)}, \quad \sigma = \sqrt{\frac{\sum_{t=1}^T \mathbb{1}(m_t = 0)(x_t - \mu)^2}{\sum_{t=1}^T \mathbb{1}(m_t = 0)}},$$

where $\mathbb{1}(\cdot)$ denotes the indicator function. These statistics are stored and applied later for Reverse Normalization to restore the predicted quantiles into the original scale of the input data. Furthermore, we follow Ansari et al. (2025) to normalize the input time series with $\bar{\mathbf{x}} = \sinh^{-1}\left(\frac{\mathbf{x} - \mu}{\sigma}\right)$,

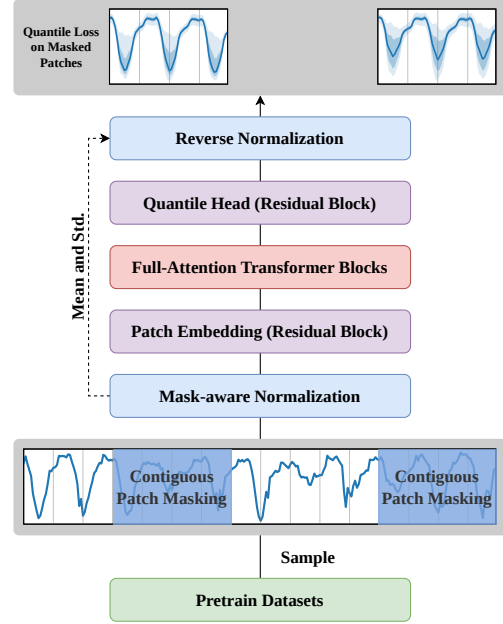


Figure 2. An overview of the generic Transformer architecture.

which suppresses the influence of extreme outliers.

3.4. Patch Embedding and Transformer Backbone

The normalized patches $\bar{\mathbf{p}}$ and the masking \mathbf{m} are projected into latent embeddings $\mathbf{h} \in \mathbb{R}^{N \times d}$ using a residual block (Das et al., 2024; Auer et al., 2025; Ansari et al., 2025), defined as

$$\mathbf{h}_{\text{out}} = f_{\text{res}}(\mathbf{h}_{\text{in}}) + f_{\text{out}}(\text{sigmoid}(f_{\text{in}}(\mathbf{h}_{\text{in}}))), \quad (1)$$

where $f_{\text{res}}, f_{\text{in}}, f_{\text{out}}$ are linear layers. Learnable positional embeddings are then added to these patch embeddings. The resulting sequence of embeddings is processed by a stack of full-attention Transformer blocks (i.e., an encoder-only Transformer) with depth N_{layer} and embedding size d . We adhere to the standard Transformer formulation with pre-normalization.

3.5. Probabilistic Prediction

To generate probabilistic predictions, we employ a Quantile Head (Auer et al., 2025; Ansari et al., 2025), implemented as a residual block, which maps the latent representations to the quantile distribution of the patches. Each patch embedding $\mathbf{h}_i \in \mathbb{R}^d$ is decoded into the normalized quantile values of the corresponding patch $\hat{\mathbf{q}}_i \in \mathbb{R}^{L \times K}$. The predictions for all patches are concatenated into $\hat{\mathbf{q}} \in \mathbb{R}^{T \times K}$. For each $q_t \in \mathbb{R}^K$, the model predicts the values for a set of quantiles levels $Q = \{\tau_1, \tau_2, \dots, \tau_K\}$.

During inference, the predicted quantiles are scaled back using the stored statistics with $y = \sinh(\hat{q}) \cdot \sigma + \mu$.

3.6. Training Objective

The model is trained to minimize the Pinball Loss (Quantile Loss), computed exclusively on the masked real values. Formally, the objective function is defined as:

$$\mathcal{L}(\hat{\mathbf{q}}, \mathbf{x}) = \frac{1}{\sum_{t=1}^T \mathbb{1}(m_t = 1)} \sum_{t=1}^T \mathbb{1}(m_t = 1) \mathcal{L}_q(\hat{\mathbf{q}}_t, x_t),$$

where $\mathcal{L}_q(\hat{\mathbf{q}}_t, x_t) = \sum_{\tau \in Q} (x_t - \hat{q}_t^{(\tau)}) \cdot (\tau - \mathbb{1}(x_t \leq \hat{q}_t^{(\tau)}))$.

(2)

Here, $\hat{q}_t^{(\tau)}$ denotes the predicted value for quantile level τ at timestamp t .

3.7. Design Analysis

Our architectural design is guided by the following core principles:

- **Simplicity:** We deliberately adhere to the generic Transformer formulation, demonstrate its effectiveness for TSFMs, and study the scaling laws in Section 5.
- **Flexibility:** Our use of CPM with randomized positions and high masking ratios prevents the model from overfitting to a specific prediction horizon, which results in flexible forecast lengths (see Figure 7). Furthermore, this generalized pretraining setting also brings the potential of extending to other tasks, such as imputation and anomaly detection.
- **Single-step Inference:** The encoder-only architecture enables parallel decoding of all target patches simultaneously. Unlike autoregressive models that generate predictions sequentially, our approach produces the entire forecast horizon in a single forward pass. This minimizes the propagation of prediction error or model’s inherent bias, and thus maximizes the role of real context from data. (See Appendix C.4.)

4. Empirical Evaluations

In this section, we rigorously evaluate the performance of our proposed architecture. We begin by detailing the experimental setup, including model hyperparameters and the composition of our pretraining corpus. Then, we demonstrate the performance of our models on probabilistic forecasting on a public benchmark.

4.1. Experiment Setups

Model Configuration: The default hyperparameters, presented in Table 6, are selected heuristically based on es-

tablished best practices in the Transformer literature. The detailed implementations are summarized in Appendix A.

Pretrain Data: A critical component of our study is the curation of a diverse and high-volume pretraining corpus. Our dataset comprises three sources:

- **Real Data:** We utilize the GIFT-Eval-Pretrain collection, consisting of 132 datasets from various domains totaling approximately 4.5 million time series and 230 billion observations.
- **KernelSynth (Synthetic):** To support long-context training ($T = 8192$), we generate 10 million univariate time series using the KernelSynth procedure (Ansari et al., 2024). As suggested by Auer et al. (2025), we employ a diverse set of periodic kernels and a small volume of augmentations.
- **TSMixup (Augmented):** To enhance temporal diversity, we incorporate TSMixup data (Ansari et al., 2024), generated by randomly mixing real-world time series. We evaluate two variants to study the impact of data leakage: (1) a “Leaky” set of 10 million series that includes samples from test-set distributions, and (2) a “Clean” set of 4 million series with all test-set overlaps removed. This comparison allows us to quantify the true zero-shot capability of the model versus performance gains from domain exposure.

Evaluated Models: Based on these data collections, we present results for two distinct model variants:

- **Zero-shot Model:** Trained on Real Data + 10M KernelSynth + 4M Clean TSMixup. This model represents a strict zero-shot setting with no exposure to test distributions.
- **Pretrained Model:** Trained on Real Data + 10M KernelSynth + 10M Leaky TSMixup. This variant serves as an upper-bound reference to demonstrate the model’s capacity when exposed to a broader, although potentially leaky, data distribution.

4.2. Benchmark Results

To assess zero-shot probabilistic forecasting performance, we utilize the GIFT-Eval benchmark (Aksu et al., 2025), a widely adopted standard for TSFMs. The benchmark encompasses 55 diverse real-world datasets spanning 97 distinct test cases, covering multiple domains of time series data and various forecast lengths.

Compared Methods: We compare our approach against the current SOTA TSFMs on the GIFT-Eval leaderboard, selecting the most recent high-performing TSFM variants, including TabPFN-TS (Hoo et al., 2024), VisionTS (Chen et al., 2025), Sundial (Liu et al., 2025), Moirai-2 (Woo et al., 2024), Toto (Cohen et al., 2025), YingLong (Wang et al., 2025), FlowState (Graf et al., 2025), TimesFM-2.5

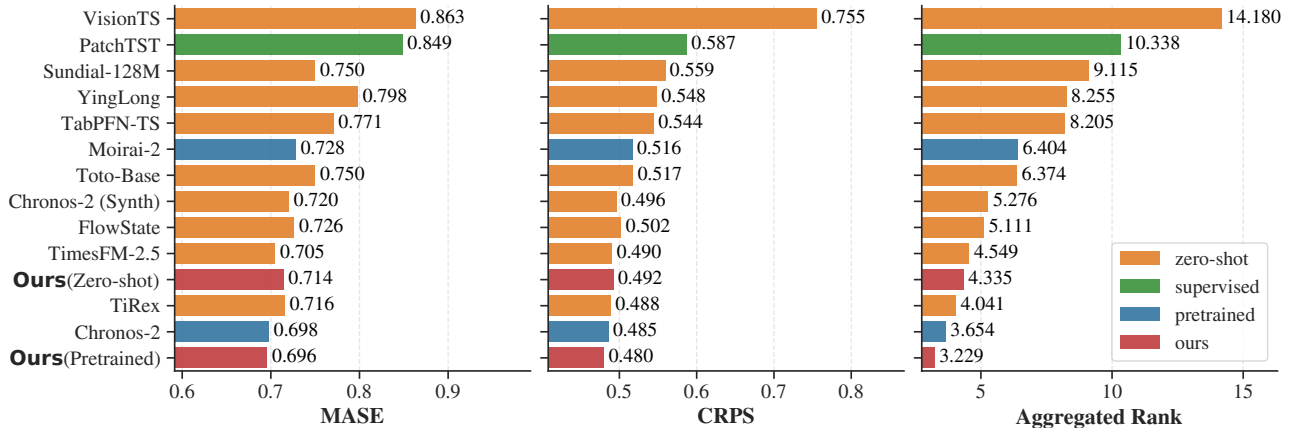


Figure 3. Forecasting performance on the GIFT-Eval benchmark. The three metrics (MASE, CRPS, Rank) are aggregated with geometric mean over the 97 test cases. Lower values indicate better performance. The methods are sorted based on Aggregated Rank.

(Das et al., 2024), Tirex (Auer et al., 2025), and Chronos-2 (Ansari et al., 2025). To provide a comprehensive context, we also include two statistical baselines (Naive and Seasonal Naive) and a supervised deep learning baseline PatchTST (Nie et al., 2023). The baseline results are obtained from the official GIFT-Eval Leaderboard. Detailed information about the baselines is summarized in Appendix B.2.

Note on Comparability: It is important to emphasize that the baseline TSFMs utilize heterogeneous training setups, varying significantly in pretraining data scale, composition, model configurations, and optimization recipes. Consequently, the benchmarking results below reflect the aggregate performance of the final model artifacts (the combination of architecture, data, and training) rather than the isolated efficacy of the architectures themselves. Our goal is not to claim architectural superiority, but to demonstrate that a generic architecture is sufficient to achieve SOTA results when coupled with a robust training recipe.

Evaluation Metrics: Following the standard GIFT-Eval protocol, we report three key metrics:

- **Mean Absolute Scaled Error (MASE):** Evaluates point forecasting accuracy by scaling the Mean Absolute Error of the predicted median (i.e., the 50th quantile $\hat{q}^{(0.5)}$) against the error of a naive forecast.
- **Continuous Ranked Probability Score (CRPS):** Assesses probabilistic forecasting quality by measuring the difference between the predicted cumulative distribution function and the ground truth observation. It effectively generalizes MAE to the probabilistic setting.
- **Rank:** Measures the relative standing of each method among all the compared methods above. Rankings are computed per-dataset based on CRPS as our primary focus on probabilistic forecasting.

Then, on each test dataset and case, the average MASE and

CRPS over all test samples are normalized w.r.t. the performance of Seasonal Naive. The metrics over the 97 cases are aggregated with geometric mean for MASE and CRPS, and arithmetic mean for Rank, as an overall evaluation of the methods on the GIFT-Eval benchmark (refer to Appendix B.1 and Aksu et al. (2025) for more details).

Results Analysis: Figure 3 summarizes the comparative performance on the GIFT-Eval benchmark. Our Pretrained model achieves the best overall results across all three metrics, while our Zero-shot variant remains highly competitive with the most recent specialized TSFMs. These findings provide strong empirical evidence that a generic Transformer architecture, when paired with a robust training recipe, is sufficient to achieve SOTA performance on time-series forecasting. Furthermore, our results demonstrate that the effective utilization of existing open-source data can yield models that match or exceed the recent TSFMs which rely on proprietary synthetic generation pipelines.

5. Systematic Ablation Study

Recognizing that the generic Transformer architecture can achieve the SOTA performance on the GIFT-Eval benchmark, we now turn to the critical question: *What are the essential drivers for this success?* As discussed in the previous sections, the heterogeneous, sometimes even opaque, training recipes of existing TSFMs often obscure whether improvements stem from architectural innovations or simply from better data and training protocols.

In this section, we conduct a large-scale ablation study to systematically breakdown these factors. We isolate and analyze the individual contributions of multiple key components. By strictly controlling variables within our standardized training pipeline, we aim to provide a transparent, empirical “recipe” for training effective TSFMs.

Throughout this section, the Rank metric is computed strictly within the context of each specific ablation experiment. For instance, when comparing a set of ablation variants (e.g., Model-A, Model-B, Model-C), their ranks are derived by comparing them against each other and the fixed set of baseline methods from Section 4.2. Consequently, the reported Rank values are relative measures intended for comparison within a specific table or figure, and should not be compared directly across different ablation studies.

5.1. Pretrain Data Composition

Table 1 investigates the impact of training data diversity on downstream performance, where we conclude the following:

- Insufficiency of Single Source:** Training on KernelSynth alone yields the poorest results, indicating that while synthetic periodic kernels capture basic seasonality, they fail to model complex real-world noise and non-stationary dynamics. Using only real data provides a stronger baseline, yet performance remains suboptimal.
- The “Synergy” Effect:** The Zero-Shot configuration, combining real and synthetic data, delivers a substantial performance boost. This suggests a complementary relationship: synthetic data acts as a robust regularizer, filling the gaps between diverse real-world distributions, while the real data provides patterns that cannot be easily synthesized.
- Benefits of Domain Exposure:** The Pretrained model, which includes the broader leaky TSMixup set, achieves the best overall performance. While the architecture generalizes well to unseen distributions (the Zero-Shot variant), exposing the model to the target domain’s patterns, even via mixed augmentations, provides an additional performance edge.

Table 1. Ablation analysis of **pretraining data composition**. We compare models trained on individual data sources and composite datasets, as introduced in Section 4.1.

Pretrain Data	MASE ↓	CRPS ↓	Rank ↓
KernelSynth	0.832	0.584	12.220
Real Only	0.790	0.542	7.008
Zero-Shot	0.714	0.492	4.591
Pretrained	0.696	0.480	3.383

Quantifying the Impact of Leakage: The performance gap between our Pretrained and Zero-Shot variants raises a critical question: *Does the leaked data merely allow the model to memorize specific test cases, or does it contribute to better feature learning?* To investigate this, we excluded all 23 leaked test cases from the benchmark and compare the models exclusively on the remaining 74 unseen cases. As illustrated in Figure 6, the Pretrained model continues to outperform the other baselines even on this clean subset.

This indicates that the inclusion of the TSMixup data did not only lead to overfitting. Instead, the increased diversity fundamentally enhanced the model’s ability to learn robust, transferable representations and predictions.

5.2. Model Scaling Laws

5.2.1. NUMBER OF PARAMETERS

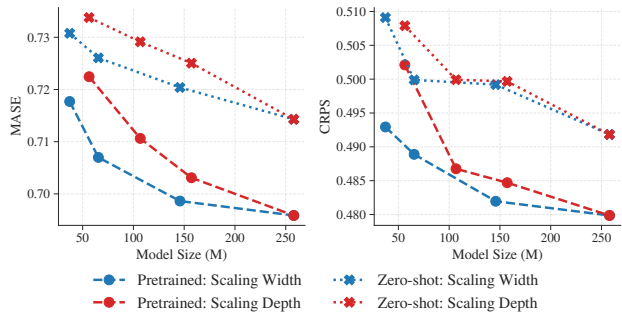


Figure 4. **Impact of model scaling on forecasting performance:** We compare increasing model capacity via embedding dimension (width) versus layer count (depth).

We investigate the impact of model capacity on forecasting accuracy by independently scaling the Transformer backbone along two axes: (1) keeping $N_{\text{layer}} = 20$ and scaling the embedding dimension $d \in \{384, 512, 768, 1024\}$, and (2) keeping $d = 1024$ and scaling the model depth $N_{\text{layer}} \in \{4, 8, 12, 20\}$. Figure 4 illustrates the scaling behavior across both MASE and CRPS metrics. We observe two key trends:

- Predictable Monotonic Scaling:** Performance improves consistently as parameter count increases, confirming that standard neural scaling laws hold for time series foundation models. This also suggests that the current architecture has not yet saturated and could benefit from further scaling.
- Depth versus Width:** At similar parameter counts, deep-narrow models consistently outperform shallow-wide models. This indicates that univariate TSFM benefits more from the hierarchical reasoning capabilities of a deep Transformer stack than from the increased feature dimension. Consequently, for parameter-efficient designs, prioritizing network depth yields better performance returns than expanding embedding size.

5.2.2. SCALING TRAINING BUDGET

We investigate the relationship between training duration and downstream performance by evaluating checkpoints throughout the pretraining process (see Figure 5). The results show a steady improvement in both MASE and CRPS. The trajectories suggest that the models have not yet reached their asymptotic limit, implying that further performance

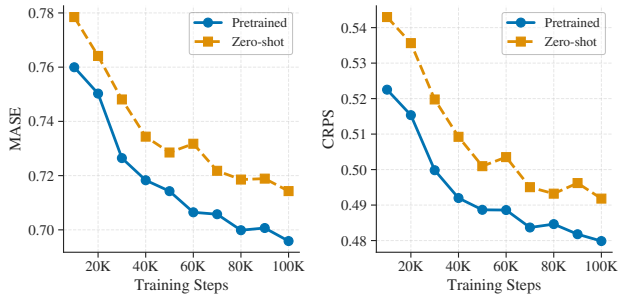


Figure 5. **Impact of training scaling on forecasting performance:** We evaluate the intermediate model checkpoints during training. MASE and CRPS for both Pretrain and Zero-shot variants exhibit a consistent monotonic improvement.

gains can be achieved simply by extending the training budget.

5.2.3. CONTEXT LENGTH

Table 2. Ablation study **input context length** on model performance. Extending the context yields significant improvements across all metrics.

Context Length	MASE ↓	CRPS ↓	Rank ↓
2048	0.721	0.500	4.592
4096	0.717	0.497	4.501
8192	0.696	0.480	3.381

We evaluate the importance of historical information by varying the input context length $T \in \{2048, 4096, 8192\}$. Table 2 demonstrates a clear benefit of scaling the lookback window on the general forecasting performance. However, we observe that these gains are most pronounced in time series that exhibit long-term seasonality (i.e., where the seasonal period is large relative to the sampling rate). In such cases, shorter lookback windows often lead to ambiguity between periodic patterns and trends, leading to suboptimal predictions. (See Figure 12 for examples)

5.2.4. OUTPUT GRANULARITY

Table 3. Ablation study on **output probability granularity**. We compare the performance of models trained to predict 9, 21, and 99 quantiles.

Num. Quantiles	MASE ↓	CRPS ↓	Rank ↓
9	0.699	0.482	3.758
21	0.700	0.481	4.087
99	0.696	0.480	3.598

We investigate the impact of the output distribution’s resolution by varying the number of predicted quantiles $K = \{9, 21, 99\}$ with the corresponding quantile levels:

- $K = 9$: $Q = \{0.1, 0.2, \dots, 0.9\}$,
- $K = 21$: $Q = \{0.01, 0.05, 0.1, \dots, 0.9, 0.95, 0.99\}$,
- $K = 99$: $Q = \{0.01, 0.02, \dots, 0.99\}$.

As shown in Table 3, the three variants result in very similar performance, while $K = 99$ has slight advantage over the coarser predictions. This indicates that while a coarse set of quantiles is sufficient to capture the general distributional, higher granularity is more general and precise for fine-grained predictions. Note that, for fair comparison, the CRPS score of the three variants are computed only on the quantile levels $\{0.1, 0.2, \dots, 0.9\}$.

5.3. Contiguous Patch Masking

Table 4. Impact of **Contiguous Patch Masking (CPM) block size**. The results show a significant performance improvement from CPM over scattered masking (i.e., $N_{\text{CPM}} = 1$).

Num. CPM	MASE ↓	CRPS ↓	Rank ↓
1	0.750	0.514	6.675
4	0.704	0.482	3.790
8	0.696	0.480	3.566

Table 5. Impact of **Masking Ratio**. The architecture remains relatively robust to this hyperparameter.

Mask Ratio	MASE ↓	CRPS ↓	Rank ↓
20%	0.698	0.484	3.900
40%	0.696	0.480	3.972
60%	0.702	0.484	4.420
80%	0.703	0.482	4.678

We analyze the design of the training objective by ablating the masking strategy, which serves as the primary mechanism for masked autoencoding, self-supervised learning. Based on results in Table 4 and Table 5, we conclude that:

- **Necessity of CPM:** Table 4 investigates the impact of the CPM block length $N_{\text{CPM}} \in \{1, 4, 8\}$. We observe that standard random patch masking (i.e., $N_{\text{CPM}} = 1$) yields poor performance. In contrast, introducing CPM significantly improves the performance by creating large “information gaps” and forcing the model to learn the underlying system dynamics for long-term predictions. Additionally, using larger N_{CPM} yields a performance edge by further pushing the model towards long-horizon understanding. (See Figure 13 for examples.)
- **Robustness to Mask Ratio:** Table 5 explores the optimal density of the masking signal. We find that the architecture is generally robust to the masking ratio, with no catastrophic failure observed even at high ratios (i.e., 80%). A ratio of 40% emerges as a “sweet spot”, achieving slightly better MASE and CRPS.

6. Discussion and Conclusion

Figure 1 visualizes the broader landscape of the capability of existing TSFMs on probabilistic forecasting, synthesizing our benchmarking results in Section 4.2 with the scaling dynamics observed in our ablations in Section 5. By comparing the performance trajectories of our generic Patch Transformer architecture against the current SOTA TSFMs, we conclude two insights regarding the current progress and direction of the field.

6.1. Architectural Progress

The scaling curves of our generic Patch Transformer show performance comparable to that of the recent SOTA TSFMs with similar sizes, matching or outperforming other deliberate architectures. This suggests that for large-scale time series modeling and pretraining, the “vanilla” Transformer architecture remains a competitive choice by demonstrating high forecasting performance and scalability. Alternatively, we also observe distinct advantages of State-Space-Models (Tirex and FlowState) which demonstrate better parameter efficiency, achieving competitive results with more compact models. Notably, FlowState achieves strong performance with *only real data from GIFT-Eval-Pretrain*, suggesting that timestamp-level modeling via SSMs may offer a valuable direction for future research. However, the scalability of SSMs has not yet been demonstrated.

6.2. Primary Drivers of Performance

In Figure 1, the vertical trajectory (purple line) reveals the profound impact of data composition on the quality and performance of TSFMs, which is further supported by Section 5.1 and Figure 6. Furthermore, our ablations in Section 5 identify that specific training techniques, especially CPM and extended context lengths, are essential mechanisms for learning dynamics of time series and performing generalized predictions. These findings suggest that the performance leaps observed in recent studies may often stem from advancements in training methodology rather than innovation in the core architecture.

6.3. Conclusion

In this work, we revisited the generic Patch Transformer to evaluate its effectiveness as a Time Series Foundation Model. We demonstrated that this generic architecture, when supported by an effective training recipe, achieves SOTA performance on the GIFT-Eval forecasting benchmark, effectively matching or exceeding the recent baseline models. Through extensive ablation studies, we disentangled the factors contributing to this success, identifying that performance is primarily driven by pretraining data composition, contiguous patch masking, and context length.

These findings imply that the rapid leaderboard advancements observed in recent TSFMs may be partially confounded by non-uniform training protocols, which obscure the actual progress in architectural innovations. By establishing this robust baseline, we highlight the dominant role of data and training techniques in current benchmarks. We hope this work encourages the community to adopt more rigorous benchmarking protocols, redirecting focus toward architectural innovations that demonstrate clear value beyond data engineering.

7. Recommendations for Future Research

Based on our findings, we make the following recommendations for the community of TSFM research:

- **Benchmark Artifact and Architecture Separately:** We distinguish between the engineering goal of releasing high-utility artifacts (i.e., model checkpoints) and the scientific goal of architectural discovery. While releasing a powerful open-source model trained on specific data is valuable for real-world practitioners, it often obscures the source of performance gains. To measure true scientific progress, we advocate for benchmarking protocols that evaluate architectures independently of their pretraining data. Future research should strive to explicitly state whether a contribution lies in a novel architectural mechanism or in a superior data curation strategy, rather than conflating the two.
- **Standardizing the Pretraining Corpus:** To enable fair architectural comparisons, the community requires a unified, publicly available pretraining corpus, analogous to ImageNet in computer vision. Currently, the heterogeneity of pretraining datasets renders cross-paper architectural comparisons virtually impossible. We advocate for the establishment of a standardized evaluation framework where models are trained on a fixed, favorably licensed, shared dataset to isolate the impact of architectural innovations from data scaling laws.
- **Bridging Research and Application with High-Quality Benchmark Datasets:** Standardized benchmarks must not come at the cost of quality of the produced artifacts. Our results demonstrate that data diversity and quality, such as the inclusion of real-world noise and broad domain coverage, are the primary drivers of model performance. Therefore, a good unified pretraining corpus should be sufficiently large and diverse to train models close to the level of “industrial production-grade” models, rather than limited “toy” datasets. By raising the quality of the standard training corpus, we should ensure that architectural improvements observed in research are robust enough to translate into meaningful gains for real-world applications.

Acknowledgements

This work was supported by IBM through the IBM-Rensselaer Future of Computing Research Collaboration (FCRC). The Authors acknowledge the National Artificial Intelligence Research Resource (NAIRR) Pilot and Mass Open Cloud for providing the computational resources contribute to this work.

Impact Statement

This paper aims to advanced Machine Learning by establishing a rigorous, performant, and open-source baseline for Time Series Foundation models. By improving the accessibility of high-performance forecasting models, our work has potential positive impacts on many essential real-world applications such as energy, supply chain, etc. We do not foresee specific negative societal consequences beyond the general risks inherent to automated decision-making systems.

References

- Aksu, T., Woo, G., Liu, J., Liu, X., Liu, C., Savarese, S., Xiong, C., and Sahoo, D. GIFT-eval: A benchmark for general time series forecasting model evaluation, 2025.
- Ansari, A. F., Stella, L., Turkmen, A. C., Zhang, X., Mercado, P., Shen, H., Shchur, O., Rangapuram, S. S., Arango, S. P., Kapoor, S., Zschiegner, J., Maddix, D. C., Wang, H., Mahoney, M. W., Torkkola, K., Wilson, A. G., Bohlke-Schneider, M., and Wang, B. Chronos: Learning the language of time series. *Transactions on Machine Learning Research*, 2024. ISSN 2835-8856.
- Ansari, A. F., Shchur, O., Küken, J., Auer, A., Han, B., Mercado, P., Rangapuram, S. S., Shen, H., Stella, L., Zhang, X., et al. Chronos-2: From univariate to universal forecasting. *arXiv preprint arXiv:2510.15821*, 2025.
- Auer, A., Podest, P., Klotz, D., Böck, S., Klambauer, G., and Hochreiter, S. Tirez: Zero-shot forecasting across long and short horizons with enhanced in-context learning. In *The Thirty-ninth Annual Conference on Neural Information Processing Systems*, 2025.
- Beck, M., Pöppel, K., Spanring, M., Auer, A., Prudnikova, O., Kopp, M. K., Klambauer, G., Brandstetter, J., and Hochreiter, S. xLSTM: Extended long short-term memory. In *The Thirty-eighth Annual Conference on Neural Information Processing Systems*, 2024.
- Chen, M., Shen, L., Li, Z., Wang, X. J., Sun, J., and Liu, C. VisionTS: Visual masked autoencoders are free-lunch zero-shot time series forecasters. In *Forty-second International Conference on Machine Learning*, 2025.
- Cohen, B., Khwaja, E., Doubli, Y., Lemaachi, S., Lettieri, C., Masson, C., Miccinilli, H., Ramé, E., Ren, Q., Ros-tamizadeh, A., du Terrail, J. O., Toon, A.-M., Wang, K., Xie, S., Xu, Z., Zhukova, V., Asker, D., Talwalkar, A., and Abou-Amal, O. This time is different: An observability perspective on time series foundation models. In *The Thirty-ninth Annual Conference on Neural Information Processing Systems*, 2025.
- Das, A., Kong, W., Sen, R., and Zhou, Y. A decoder-only foundation model for time-series forecasting. In *Forty-first International Conference on Machine Learning*, 2024.
- Devlin, J., Chang, M.-W., Lee, K., and Toutanova, K. Bert: Pre-training of deep bidirectional transformers for language understanding. In *Proceedings of the 2019 conference of the North American chapter of the association for computational linguistics: human language technologies, volume 1 (long and short papers)*, pp. 4171–4186, 2019.
- Dosovitskiy, A., Beyer, L., Kolesnikov, A., Weissenborn, D., Zhai, X., Unterthiner, T., Dehghani, M., Minderer, M., Heigold, G., Gelly, S., Uszkoreit, J., and Houshy, N. An image is worth 16x16 words: Transformers for image recognition at scale. In *International Conference on Learning Representations*, 2021.
- Emami, P., Sahu, A., and Graf, P. Buildingsbench: A large-scale dataset of 900k buildings and benchmark for short-term load forecasting. In *Thirty-seventh Conference on Neural Information Processing Systems Datasets and Benchmarks Track*, 2023.
- Godahewa, R. W., Bergmeir, C., Webb, G. I., Hyndman, R., and Montero-Manso, P. Monash time series forecasting archive. In *Thirty-fifth Conference on Neural Information Processing Systems Datasets and Benchmarks Track (Round 2)*, 2021.
- Goswami, M., Szafer, K., Choudhry, A., Cai, Y., Li, S., and Dubrawski, A. Moment: A family of open time-series foundation models. In *International Conference on Machine Learning*, 2024.
- Graf, L., Ortner, T., Woł̧śniak, S., Pantazi, A., et al. Flow-state: Sampling rate invariant time series forecasting. *arXiv preprint arXiv:2508.05287*, 2025.
- He, K., Chen, X., Xie, S., Li, Y., Dollár, P., and Girshick, R. Masked autoencoders are scalable vision learners. In *Proceedings of the IEEE/CVF conference on computer vision and pattern recognition*, pp. 16000–16009, 2022.
- Hoo, S. B., Müller, S., Salinas, D., and Hutter, F. The tabular foundation model tabPFN outperforms specialized time series forecasting models based on simple features.

- In *NeurIPS 2024 Third Table Representation Learning Workshop*, 2024.
- Howard, A., Yui, H., McDonald, M., and Cukierski, W. Recruit restaurant visitor forecasting. <https://kaggle.com/competitions/recruit-restaurant-visitor-forecasting>, 2017. Kaggle.
- Jiang, J., Han, C., Jiang, W., Zhao, W. X., and Wang, J. Libcity: A unified library towards efficient and comprehensive urban spatial-temporal prediction. *arXiv preprint arXiv:2304.14343*, 2023.
- Kim, T., Kim, J., Tae, Y., Park, C., Choi, J.-H., and Choo, J. Reversible instance normalization for accurate time-series forecasting against distribution shift. In *International Conference on Learning Representations*, 2022.
- Lai, G., Chang, W.-C., Yang, Y., and Liu, H. Modeling long-and short-term temporal patterns with deep neural networks. In *The 41st international ACM SIGIR conference on research & development in information retrieval*, pp. 95–104, 2018.
- Liu, X., Xia, Y., Liang, Y., Hu, J., Wang, Y., Bai, L., Huang, C., Liu, Z., Hooi, B., and Zimmermann, R. LargeST: A benchmark dataset for large-scale traffic forecasting. In *Thirty-seventh Conference on Neural Information Processing Systems Datasets and Benchmarks Track*, 2023.
- Liu, Y., Qin, G., Shi, Z., Chen, Z., Yang, C., Huang, X., Wang, J., and Long, M. Sundial: A family of highly capable time series foundation models. In *Forty-second International Conference on Machine Learning*, 2025.
- Nguyen, T., Jewik, J. K., Bansal, H., Sharma, P., and Grover, A. Climatelearn: Benchmarking machine learning for weather and climate modeling. In *Thirty-seventh Conference on Neural Information Processing Systems Datasets and Benchmarks Track*, 2023.
- Nie, Y., H. Nguyen, N., Sinthong, P., and Kalagnanam, J. A time series is worth 64 words: Long-term forecasting with transformers. In *International Conference on Learning Representations*, 2023.
- Palaskar, S., Ekambaram, V., Jati, A., Gantayat, N., Saha, A., Nagar, S., Nguyen, N. H., Dayama, P., Sindhgatta, R., Mohapatra, P., et al. Automixer for improved multivariate time-series forecasting on business and it observability data. In *Proceedings of the AAAI conference on artificial intelligence*, volume 38, pp. 22962–22968, 2024.
- Shen, S., Van Beek, V., and Iosup, A. Statistical characterization of business-critical workloads hosted in cloud datacenters. In *2015 15th IEEE/ACM international symposium on cluster, cloud and grid computing*, pp. 465–474. IEEE, 2015.
- Shi, X., Wang, S., Nie, Y., Li, D., Ye, Z., Wen, Q., and Jin, M. Time-moe: Billion-scale time series foundation models with mixture of experts. In *The Thirteenth International Conference on Learning Representations*, 2025.
- Smith, J. T., Warrington, A., and Linderman, S. Simplified state space layers for sequence modeling. In *The Eleventh International Conference on Learning Representations*, 2023.
- Trindade, A. ElectricityLoadDiagrams20112014. UCI Machine Learning Repository, 2015. DOI: <https://doi.org/10.24432/C58C86>.
- Vaswani, A., Shazeer, N., Parmar, N., Uszkoreit, J., Jones, L., Gomez, A. N., Kaiser, L., and Polosukhin, I. Attention is all you need. In *Advances in Neural Information Processing Systems*, volume 30, 2017.
- Wang, X., Zhou, T., Gao, J., Ding, B., and Zhou, J. Output scaling: Yinglong-delayed chain of thought in a large pretrained time series forecasting model. *arXiv preprint arXiv:2506.11029*, 2025.
- Wen, Y., Ma, T., Weng, T.-W., Nguyen, L. M., and Julius, A. A. Abstracted shapes as tokens - a generalizable and interpretable model for time-series classification. In *The Thirty-eighth Annual Conference on Neural Information Processing Systems*, 2024.
- Woo, G., Liu, C., Kumar, A., Xiong, C., Savarese, S., and Sahoo, D. Unified training of universal time series forecasting transformers. In *Forty-first International Conference on Machine Learning*, 2024.
- Wu, H., Xu, J., Wang, J., and Long, M. Autoformer: Decomposition transformers with auto-correlation for long-term series forecasting. In *Advances in Neural Information Processing Systems*, 2021.
- Zhou, H., Zhang, S., Peng, J., Zhang, S., Li, J., Xiong, H., and Zhang, W. Informer: Beyond efficient transformer for long sequence time-series forecasting. In *Proceedings of the AAAI conference on artificial intelligence*, volume 35, pp. 11106–11115, 2021.

A. Implementation Details

A.1. Experiment Framework

Our models, training pipeline, and experiments are implemented using PyTorch and the Hugging Face ecosystem. To ensure broad compatibility with open-source frameworks, we leverage standard libraries including the `PretrainedModel` class, `Trainer`, `Accelerate`, and `Datasets`. All pretraining experiments were conducted on NVIDIA V100 GPUs using FP16 mixed-precision training to optimize computational efficiency.

A.2. Hyperparameters

Table 6. Detailed Hyperparameter Configuration. The values are selected based on standard practices in TSFMs and Transformers.

Hyperparameter	Value	Rationale / Source
Architecture		
Context Length (T)	8192	A large context window for general usage. (Ansari et al., 2025)
Patch Size (L)	16	Standard choice for patch size. (Dosovitskiy et al., 2021)
Number of Layers (N_{layer})	20	Modified from ViT-Large.
Embedding Dimension (d)	1024	From ViT-Large.
Attention Head Dimension	64	Standard choice for Transformers.
Number of Attention Heads	$d/64$	Standard choice for Transformers.
Number of Quantiles (K)	99	
Quantile Levels Q	$\{0.01, 0.02, \dots, 0.99\}$	
Training Configurations		
Masking Ratio	40%	An intermediate value based on BERT (Devlin et al., 2019) and MAE (He et al., 2022).
CPM Block Size (N_{cpm})	8	
Optimization		
Total Training Steps	100k	
Effective Batch Size	2048	
Optimizer	AdamW	Standard choice for foundation models.
Learning Rate Schedule	Cosine with Linear Warmup	Standard choice for foundation models.
Peak Learning Rate	$3 \cdot 10^{-4}$	Standard choice, conservative for training stability.
Minimum Learning Rate	$1 \cdot 10^{-5}$	
Weight Decay	0.1	Empirical choice to ensure training stability.
(β_1, β_2) in AdamW	(0.9, .95)	Empirical choice to ensure training stability.
Gradient Norm Clipping	1	Standard choice, conservative for training stability.
Precision	FP16 Mixed	Accelerate training, supported by V100 GPUs.

A.3. Masking Strategy

We provide supplementary details regarding the input processing described in Section 3. The design of the input mask is critical for ensuring model flexibility and generalized usage.

Mask Processing In our implementation, the unified input mask \mathbf{m} is a composite of three distinct components:

- Prediction mask \mathbf{m}^{pred} : Designates the observed values in the sequence that are dropped to serve as prediction targets. To optimize the model for forecasting tasks, we randomly mask $\mathcal{U}(0, 4 \cdot N_{\text{CPM}})$ timestamps at the end of each training sample in addition to CPMs at random locations.
- Missing mask \mathbf{m}^{miss} : Identifies inherent missing values within the raw data. These values are retained in the attention mechanism (to preserve temporal position) but are marked as missing in \mathbf{m} and strictly excluded from the loss

calculation.

- Padding mask \mathbf{m}^{pad} : Identifies padding tokens used to fill the context window when the input sequence length is shorter than the context window T . We apply left-padding to align the sequence. Patches consisting entirely of padding values are masked out of the attention mechanism, where we empirically find this approach could improve performance by saving attention.

The model processes the logical union of these masks, defined as $\mathbf{m} = \mathbf{m}^{\text{pred}} \vee \mathbf{m}^{\text{miss}} \vee \mathbf{m}^{\text{pad}}$. Note that in Section 3 and Equation 2, we simplified the notation to assume $\mathbf{m} \approx \mathbf{m}^{\text{pred}}$ for clarity of presentation.

Adaptive Contiguous Patch Masking CPM masks blocks of $N_{\text{CPM}} \cdot L$ consecutive observations. However, applying a fixed block size to short input sequences can inadvertently mask the entire valid history. Therefore, we implement an Adaptive CPM strategy. Formally for a time series $\mathbf{x} \in \mathbb{R}^{T^{(x)}}$ with length $T^{(x)} \ll T$, we dynamically adjust the block size $N_{\text{CPM}}^{(x)}$ as follows:

$$N_{\text{CPM}}^{(x)} = \min \left(\left\lceil \frac{\lceil T^{(x)} / L \rceil}{4} \right\rceil, N_{\text{CPM}} \right).$$

This preserves sufficient context for the model to learn meaningful dependencies even in short samples.

B. Benchmark and Baselines

B.1. GIFT-Eval

Evaluation Metrics Here, we provide the detailed formulations of the GIFT-Eval metrics.

MASE is a metric for point forecasting. It compares the prediction’s absolute error against the mean absolute error of a Naive forecasting baseline. Formally, given the target $\mathbf{x} \in \mathbb{R}^T$ and predicted median $\hat{\mathbf{q}}^{(0.5)} \in \mathbb{R}^T$, the MASE is calculated as follows:

$$\text{MASE}(\hat{\mathbf{q}}^{(0.5)}, \mathbf{x}) = \frac{\frac{1}{T} \sum_{t=1}^T |x_t - \hat{q}^{(0.5)}|}{\frac{1}{T-1} \sum_{t=2}^T |x_t - x_{t-1}|}. \quad (3)$$

CRPS evaluates the accuracy of probabilistic forecasts. CRPS measures the difference between the predicted cumulative distribution functions (CDFs) and the target values. In practice, computing the CDFs via integration is computationally expensive. The GIFT-Eval benchmarking protocol approximates the CRPS using a discrete sum over a finite set of quantile levels, often referred to as the mean weighted quantile loss.

Let $\hat{\mathbf{q}} \in \mathbb{R}^{T \times K}$ denote the predicted values for the quantile levels $Q = \{\tau_1, \dots, \tau_K\}$. The approximated CRPS is defined as follows:

$$\text{CRPS}(\hat{\mathbf{q}}, \mathbf{x}) \approx \frac{1}{K} \sum_{k=1}^K \text{wQL}[\tau_k], \text{ where } \text{wQL}[\tau_k] = 2 \frac{\sum_{t=1}^T (\tau - \mathbb{1}(x_t < \hat{q}_t^{(\tau)}))(x_t - \hat{q}_t^{(\tau)})}{\sum_{t=1}^T |x_t|}. \quad (4)$$

Dataset Information The GIFT-Eval benchmark contains 55 datasets from 7 macro domains, including Nature, Web and Cloud Applications, Sales, Energy, Transportation, Economy and Finance, and Healthcare. The datasets are obtained from popular time series forecasting benchmarks, including Informer (Zhou et al., 2021), Autoformer (Wu et al., 2021), AutoMixer (Palaskar et al., 2024), LibCity (Jiang et al., 2023), LSTNet (Lai et al., 2018), Monash Archive (Godaheva et al., 2021), Grid Workloads Archive (Shen et al., 2015), and Restaurant Competition (Howard et al., 2017), and UCI ML Archive (Trindade, 2015). Please refer to Aksu et al. (2025) for the detailed information about the GIFT-Eval and GIFT-Eval-Pretrain datasets.

B.2. Baselines

Table 7. Comparison of recent foundation models. Pretraining corpora sources are summarized for brevity. Publicly-available data are highlighted with blue. Corpus overlap with the GIFT-Eval test cases are highlighted with red.

Model	Size	Arch.	Context Len.	Pretrain Corpus
TabPFN-TS (Hoo et al., 2024)	11M	Encoder	4096 ⁽¹⁾	Synthetic (Gaussian Process, Structured Causal Models).
Sundial (Liu et al., 2025)	128M	Decoder	2880	Subset of Chronos, LOTSA, Synthetic, Finance, IoT.
YingLong (Wang et al., 2025)	300M	Encoder	8192	Subset of Chronos, KernelSynth.
Moirai-2 (Woo et al., 2024)	14M	Encoder	512	GIFT-Eval-Pretrain, Training split of GIFT-Eval, TSMixup, KernelSynth, Internal Operations Data. Curated to remove the “low-quantity” samples.
Toto (Cohen et al., 2025)	151M	Decoder	4096	Observability Metrics, GIFT-Eval-Pretrain, Subset of Chronos, Synthetic.
FlowState (Graf et al., 2025)	9.1M	S5	2048	GIFT-Eval-Pretrain.
TimesFM-2.5 (Das et al., 2024)	200M	Decoder	16384	GIFT-Eval-Pretrain, Wiki Pageviews, Google Trends, Synthetic.
Tirex-1.1 (Auer et al., 2025)	35M	xLSTM	2048 ⁽²⁾	Subset of GIFT-Eval-Pretrain, Subset of Chronos, Synthetic.
Chronos-2 (Ansari et al., 2025)	120M	Encoder	8192	Chronos, High-volume Synthetic.

Table 7 summarizes the key specifications of the baseline Time Series Foundation Models (TSFMs) evaluated in this study, including model size, backbone architecture, context length, and pretraining corpus composition. This information was collated from the original publications, official GitHub repositories, and Hugging Face model cards. We note the following specific configurations:

1. **TabPFN:** While the model supports variable input lengths, we report a context length of 4096, consistent with the default setting in the official evaluation code.
2. **Tirex:** We report the context length of 2048 based on the initial version described in Auer et al. (2025). Although Tirex-1.1 introduces updates to address data leakage in the original release and some improvements, the context length is not explicitly redefined in the documentation; we therefore assume it remains unchanged.
3. **Synthetic Data:** The inclusion of synthetic data has become a standard practice for pretraining TSFMs. Notably, many recent works generate their own synthetic corpora. While the generation methodologies are often briefly described in technical reports or publications, the exact synthetic datasets are rarely released.

C. Addition Experiment Results and Visualizations

C.1. Additional Benchmarking Results

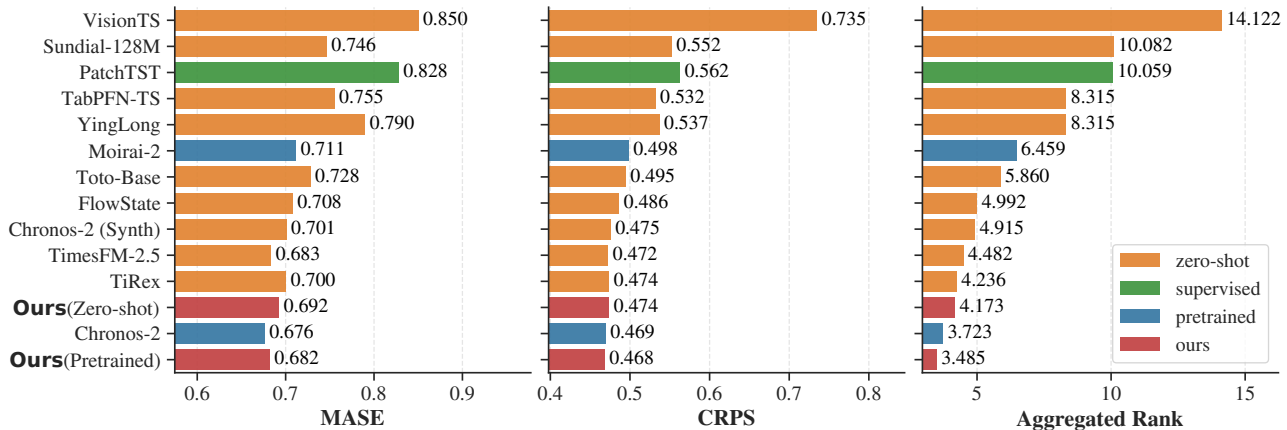


Figure 6. Zero-shot forecasting performance on the GIFT-Eval benchmark. The three metrics (MASE, CRPS, Rank) are aggregated with geometric mean over the 74 non-leaky test cases. Lower values indicate better performance. The methods are sorted based on Aggregated Rank.

C.2. When will it fail? Explore the maximum supported forecast length

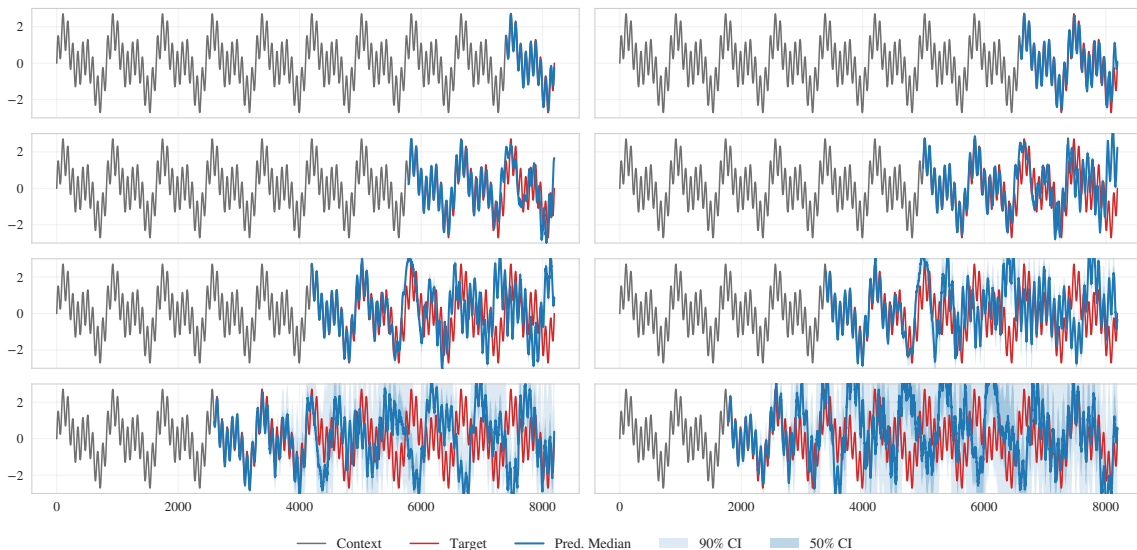


Figure 7. Examples of predictions on a synthetic signal with different prediction lengths.

Our generalized pretraining masking strategy offers the distinct advantage of flexible forecast lengths. In Figure 7, we investigate the effective maximum forecasting horizon supported by the model. We evaluate performance on a synthetic multi-frequency sine wave across forecast lengths $\{800, 1600, \dots, 6400\}$. We observe that while predictions remain accurate for shorter horizons $\{800, 1600\}$, performance gradually degrades as the forecast length increases. These findings imply the following:

- For optimal performance, the maximum reliable forecast length is approximately 2000 timestamps. Extending beyond this limit can be achieved with autoregressive decoding.
- Neural models may struggle to extrapolate "simple" periodic cases over long horizons, whereas such patterns are often trivially predicted by classical statistical models.

C.3. Visualizations of Predictions

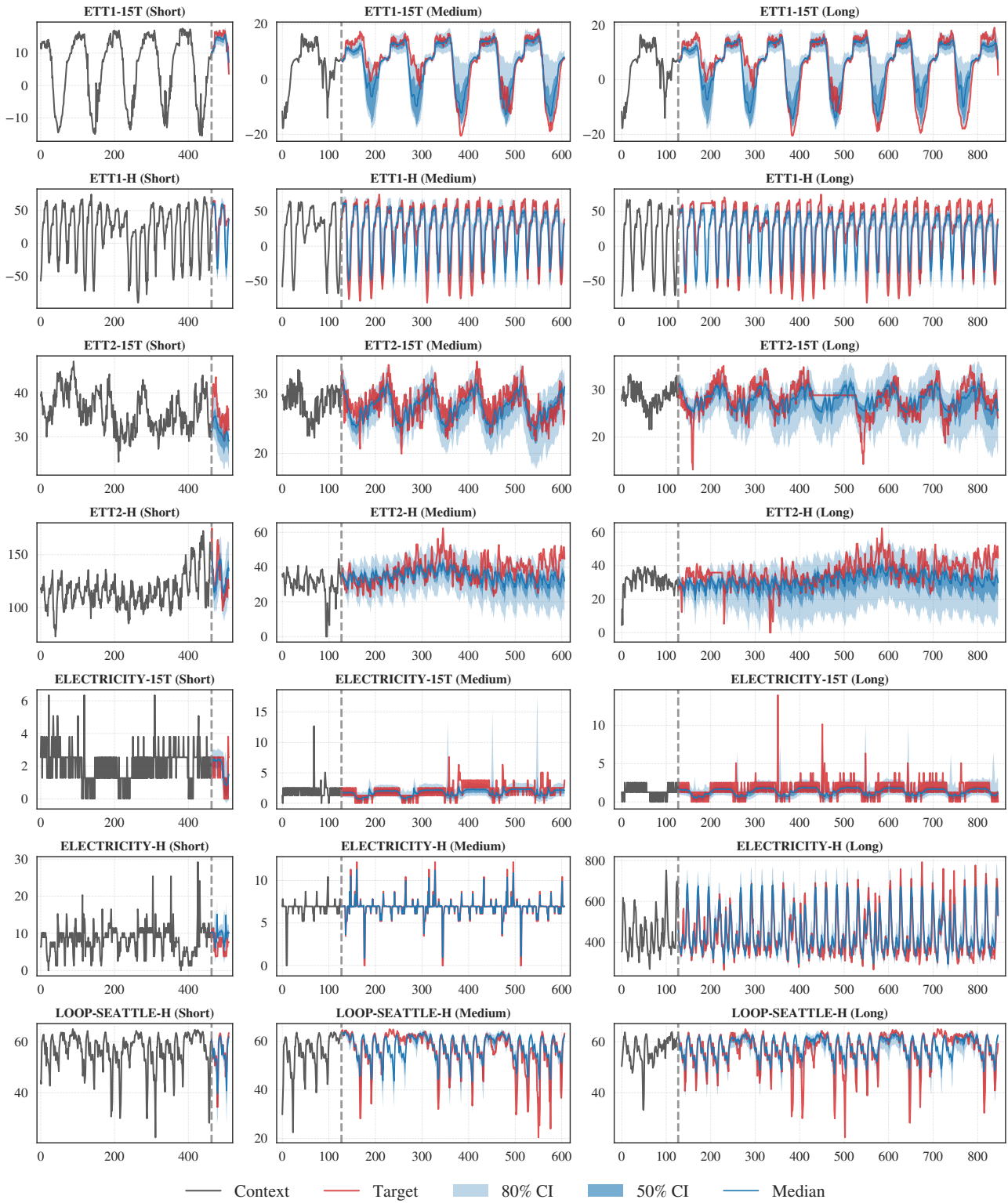


Figure 8. Examples of predictions from our **Pretrained** model on datasets with significant seasonal patterns.

Revisiting the Generic Transformer: Deconstructing a Strong Baseline for Time Series Foundation Models

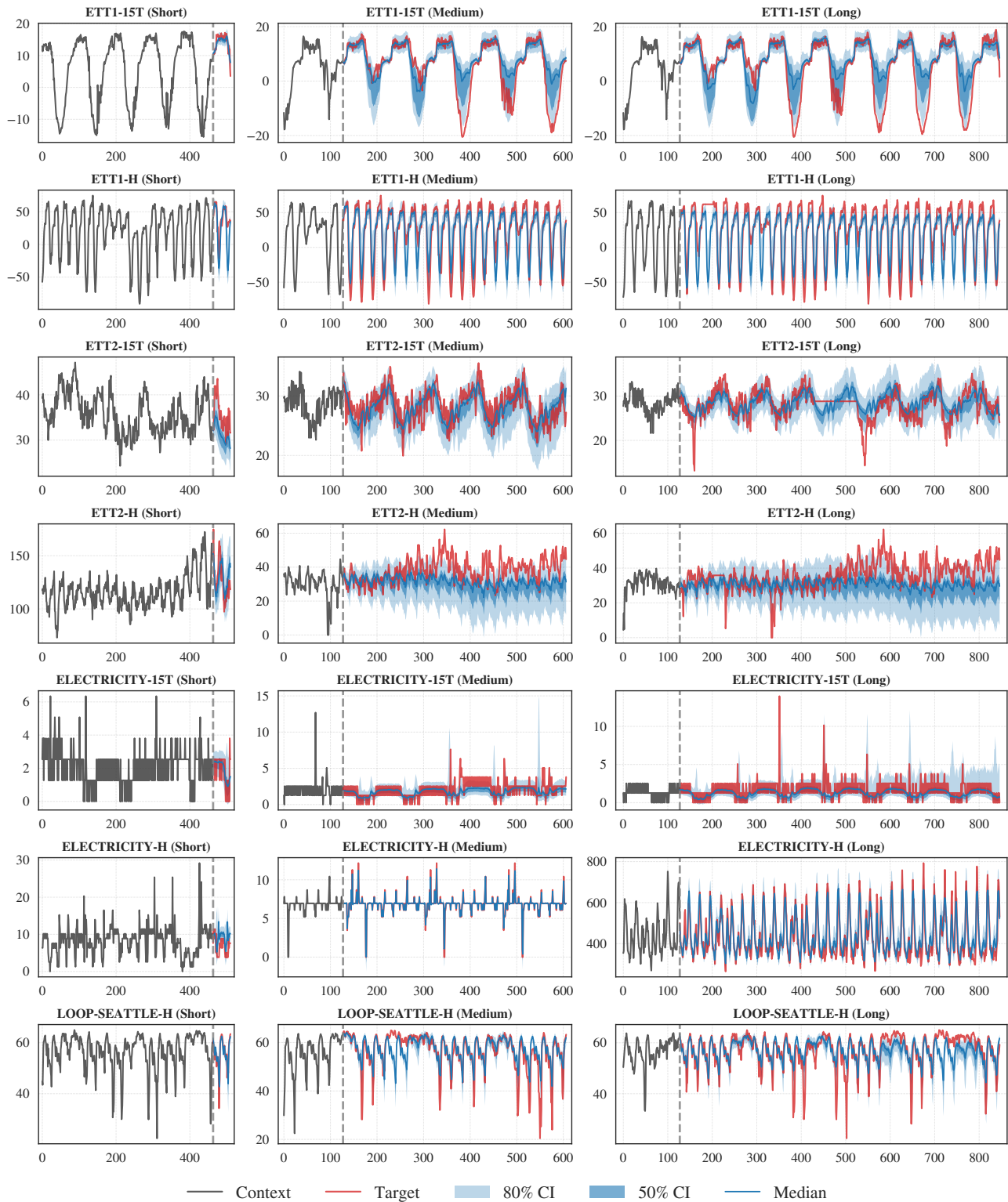


Figure 9. Examples of predictions from our **Zero-shot** model on datasets with significant seasonal patterns.

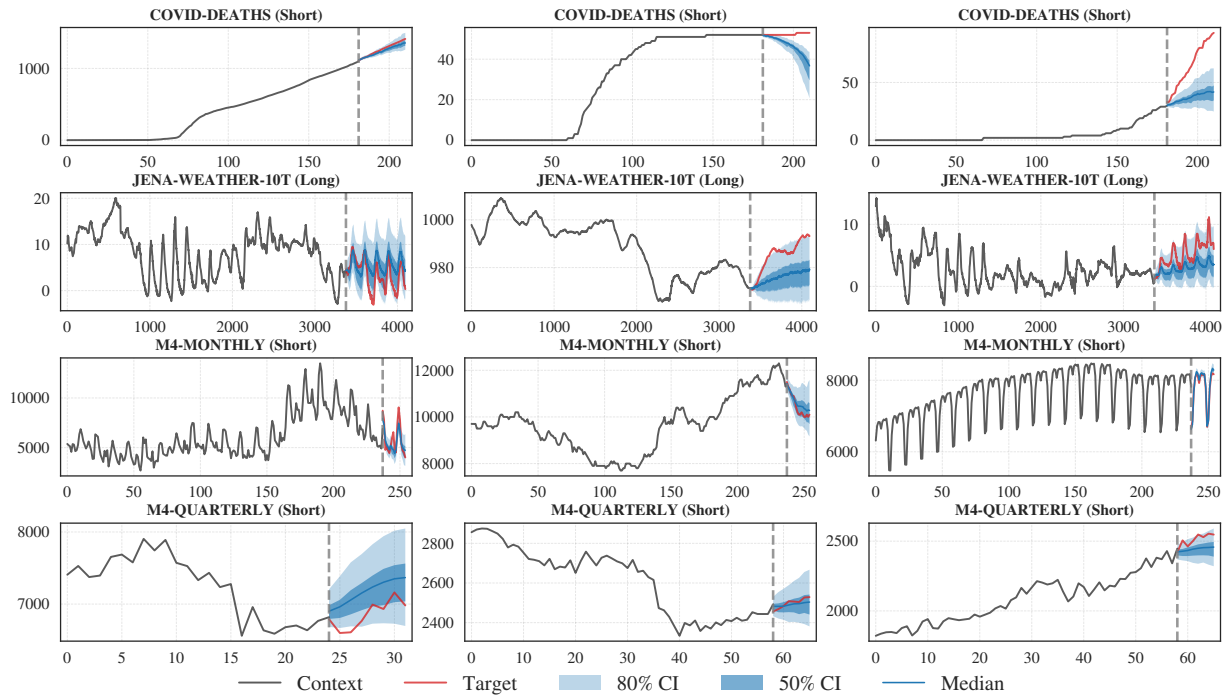


Figure 10. Examples of predictions from our **Pretrained** model on datasets with significant trend patterns.

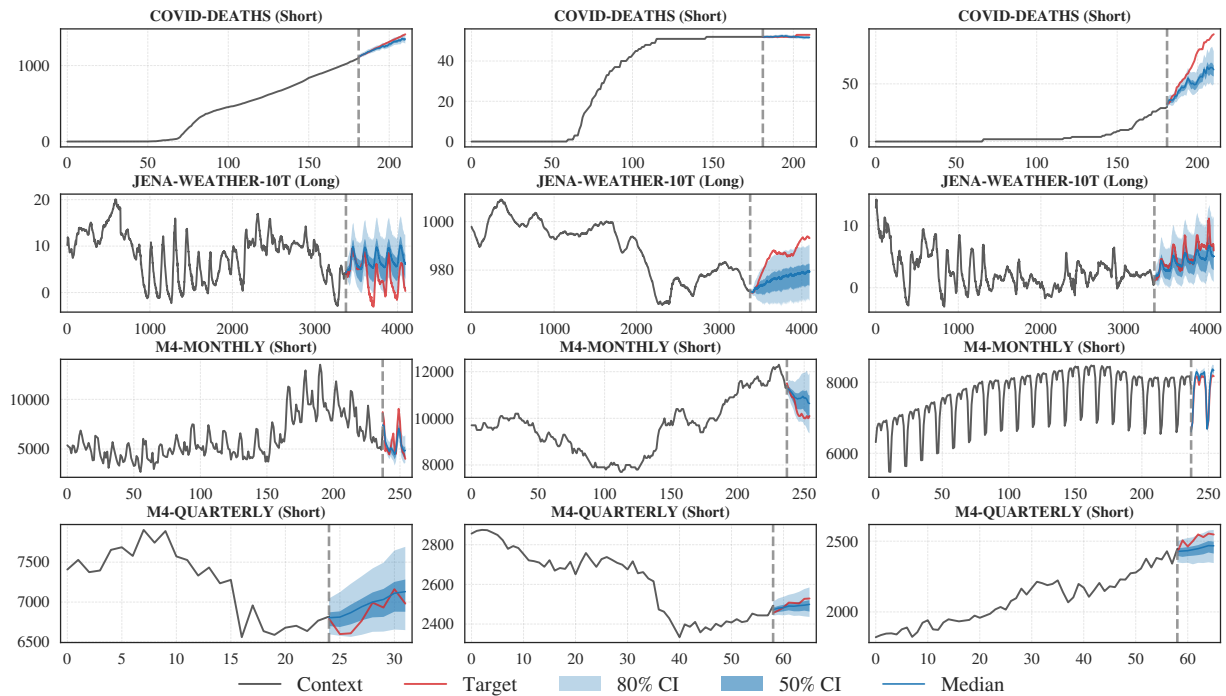


Figure 11. Examples of predictions from our **Zero-shot** model on datasets with significant trend patterns.

Revisiting the Generic Transformer: Deconstructing a Strong Baseline for Time Series Foundation Models

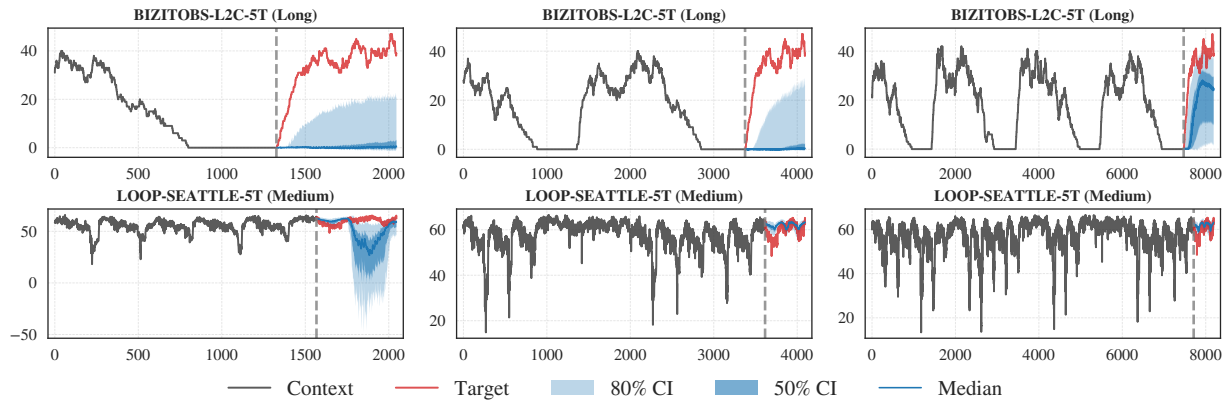


Figure 12. Example of the predictions from models with context length (left) 2048, (middle) 4096, and (right) 8192. Shorter context lengths may fail to capture periodicity and produce poor forecasts, while longer context lengths is more robust for general usage.

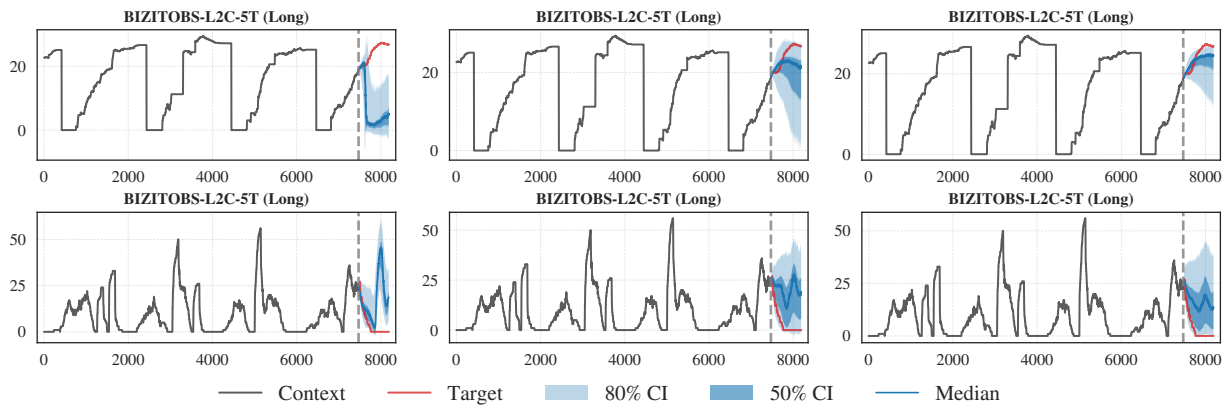


Figure 13. Examples of the predictions from models pretrained with CPM Block Size (left) $N_{\text{CPM}} = 1$, (middle) $N_{\text{CPM}} = 4$, and (right) $N_{\text{CPM}} = 8$. Larger N_{CPM} encourages the model to infer the underlying time series dynamics, providing better forecasts for general usage.

C.4. Inference Time

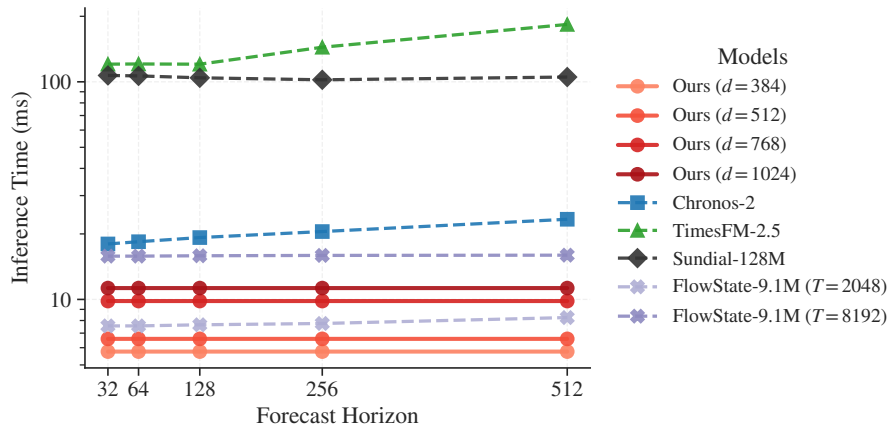


Figure 14. Inference time of our models and other TSFMs. Benefit from high mask ratio, single-step inference, and architecture simplicity, our models also excel in inference time which is invariant to the forecast horizon.

Figure 14 benchmarks the inference latency of our proposed architecture against state-of-the-art TSFMs. All evaluations were conducted on an NVIDIA RTX 6000 Blackwell GPU using a batch size of 1. To ensure a rigorous comparison, we set the input context length to $T = 8192$ for all compatible models, while adjusting for architectural constraints in baselines such as Sundial ($T = 2880$). While FlowState is pretrained with $T = 2048$, it also supports longer context length as a state-space model. Therefore, we include the evaluation for both cases and compare their inference speed. Results for comparison models were derived using their official implementations for inference. We note that Tires is excluded from this specific comparison due to hardware-specific compilation incompatibilities with its custom state-space model kernels.